Ehsan Ban
Department of Mechanical, Aerospace,
and Nuclear Engineering,
Rensselaer Polytechnic Institute,
Jonsson Engineering Center, Room 2049,
110 8th Street,
Troy, NY 12180;
Scientific Computation Research Center,
Rensselaer Polytechnic Institute,
Low Center for Industrial Innovation,
CII-4011 110 8th Street,
Troy, NY 12180
e-mail: bane@rpi.edu

Victor H. Barocas
Department of Biomedical Engineering,
University of Minnesota,
7-105 Nils Hasselmo Hall,
312 Church Street SE,
Minneapolis, MN 55455
e-mail: baroc001@umn.edu

Mark S. Shephard
Scientific Computation Research Center,
Rensselaer Polytechnic Institute,
Low Center for Industrial Innovation,
CII-4011 110 8th Street,
Troy, NY 12180
e-mail: shephard@rpi.edu

Catalin R. Picu[1]
Department of Mechanical,
Aerospace, and Nuclear Engineering,
Rensselaer Polytechnic Institute,
Jonsson Engineering Center, Room 2048,
110 8th Street,
Troy, NY 12180;
Scientific Computation Research Center,
Rensselaer Polytechnic Institute,
Low Center for Industrial Innovation,
CII-4011 110 8th Street,
Troy, NY 12180
e-mail: picuc@rpi.edu

Effect of Fiber Crimp on the Elasticity of Random Fiber Networks With and Without Embedding Matrices

Fiber networks are assemblies of one-dimensional elements representative of materials with fibrous microstructures such as collagen networks and synthetic nonwovens. The mechanics of random fiber networks has been the focus of numerous studies. However, fiber crimp has been explicitly represented only in few cases. In the present work, the mechanics of cross-linked networks with crimped athermal fibers, with and without an embedding elastic matrix, is studied. The dependence of the effective network stiffness on the fraction of nonstraight fibers and the relative crimp amplitude (or tortuosity) is studied using finite element simulations of networks with sinusoidally curved fibers. A semi-analytic model is developed to predict the dependence of network modulus on the crimp amplitude and the bounds of the stiffness reduction associated with the presence of crimp. The transition from the linear to the nonlinear elastic response of the network is rendered more gradual by the presence of crimp, and the effect of crimp on the network tangent stiffness decreases as strain increases. If the network is embedded in an elastic matrix, the effect of crimp becomes negligible even for very small, biologically relevant matrix stiffness values. However, the distribution of the maximum principal stress in the matrix becomes broader in the presence of crimp relative to the similar system with straight fibers, which indicates an increased probability of matrix failure.
[DOI: 10.1115/1.4032465]

1 Introduction

Fiber networks are assemblies of one-dimensional elements that can be used to model the mechanics of fibrous materials. The first such models were developed for paper and paper products, and a large literature exists on the subject (see Ref. [1] for a review). In the last two decades, random fiber networks have been used to represent assemblies of semiflexible filaments, i.e., filaments in which the bending stiffness of fibers is not negligible, encountered in biological materials. The structural element of all connective tissues contains as the primary element a network of collagen and elastin. This pervasiveness of network structures in biomaterials and biological structures stimulated an intense activity in this area, activity which continues today. A review of these efforts is provided in Ref. [2].

The central goal of these efforts has been to understand the relationship between the network structure and its mechanical behavior. When subjected to uniaxial tension or shear, a cross-linked random fiber network exhibits an initial linear elastic deformation regime, followed at larger strains by a nonlinear elastic response [3–5]. The initial regime is characterized by the elastic modulus, E_N. In the nonlinear range, the tangent stiffness is related to the stress through a power law function [3]. The strain range in which the power law applies is bounded by the strain at which the nonlinear range begins and by another critical strain at which other processes, such as failure, activation of unfolding in cross-linking proteins, or full fiber alignment, are triggered [3,5].

The small-strain elastic modulus E_N was related to the network parameters in a number of studies [1,6,7]. It is now well-established that in networks made from the same type of fibers, an important role is played by a parameter with units of length, $l_b = \sqrt{(EI)_f/(EA)_f}$, where $(EA)_f$ and $(EI)_f$ are parameters that determine the axial and bending stiffness of fibers, $(EA)_f/l$ and $(EI)_f/l^3$ (here l is the length of an individual fiber). When $l_b \gg \bar{l}$, where $\bar{l}$ is the mean fiber segment length, the network modulus is

[1]Corresponding author.

Contributed by the Applied Mechanics Division of ASME for publication in the Journal of Applied Mechanics. Manuscript received November 9, 2015; final manuscript received January 11, 2016; published online January 27, 2016. Assoc. Editor: M. Taher A. Saif.

proportional to $(EA)_f$, while in networks with $l_b \ll \bar{l}$, the network modulus is proportional to $(EI)_f$. These limits are denoted as the axial- and bending-dominated regimes, respectively. The network modulus, E_N, is proportional to the density of the network, ρ, in the axial-dominated regime and scales as ρ^{α} in the bending-dominated range. Various values of α between 2 and 8 have been reported depending on the network structure and the dimensionality of the embedding space (2D versus 3D) [8,9].

Most networks of interest, such as the collagen networks in connective tissue or fibrin networks in blood clots, are embedded in a matrix. The effect of the matrix on the mechanics of the composite has been studied recently [10,11]. The usual modeling procedure in the biomechanics literature is to decouple the two components and consider that the matrix and network are subjected to the same boundary conditions but deform independently [12,13]. A coupled model was developed by Zhang et al. [11], in which the compatibility of the deformation field is ensured at all points of each fiber of the model. This study indicates that in soft tissue, the matrix and network interact strongly, with the matrix reducing the degree of nonaffinity of the deformation field of the network. In turn, this leads to a highly heterogeneous stress field in the matrix material.

Curved (crimped) athermal fibers are encountered in both biological and synthetic unloaded networks. For example, different levels of crimp/tortuosity have been reported for in vivo collagen fibrils, depending on age [14] and anatomical location [15]. Also, fiber tortuosity is ubiquitous in nonwovens used for various consumer products such as absorbent and insulating materials. Various models have been developed to account for the crimp effect in fibrous networks [5,16–18]. The simplest models assume that fibers are straight, but their response to stretch is modified and includes an initial regime, the crimp pull-out regime, in which the deformation takes place at zero or very small axial force [12,16,18]. This effective constitutive behavior of the fibers can be derived based on the response of the actual, crimped fibers to stretch [4,17]. The prediction of the behavior of the network of curved fibers can then be made either using the assumption of affine deformation of the network, and hence the fiber end-to-end vectors [12,18], or using a detailed network model.

Kabla and Mahadevan [17] performed experiments on synthetic polyester felts, in which the majority of fibers are crimped, and related the fiber and network behaviors using a reduced-order representative network model with six fibers. They explicitly account for fiber crimp statistics, which is used to evaluate the constitutive behavior of the fibers in the representative model. Onck et al. [5] and Huisman et al. [18] studied cross-linked networks of curved athermal fibers numerically. They introduce fiber initial curvature by using thermal statistical chain models and by controlling the chain persistence length. It is observed that at small strains, fiber crimp leads to softer responses while the stress–strain curves converge to the same asymptote at larger strains when the fiber undulations are straightened.

Motivated by the observations of significant deformation nonaffinity in the mechanics of biopolymers [19], this work addresses the effect of crimp on the nonaffine deformation of athermal cross-linked networks with and without matrix. Networks with different crimp amplitudes and fractions of crimped fibers are considered and a quantitative relationship is established between these two parameters and E_N. To the best of our knowledge, this is the first analytical model to explain the reduction of stiffness in the presence of crimp for a network without any assumption about the deformation field. The response to large deformations of networks of crimped fibers is also studied. Additionally, the effect of the matrix is accounted for by explicitly imposing the fiber-matrix deformation compatibility in the spirit of the model of Zhang et al. [10]. Section 2 outlines the model and solution procedure, while the results and discussion are presented in Sec. 3 for both nonembedded and embedded networks.

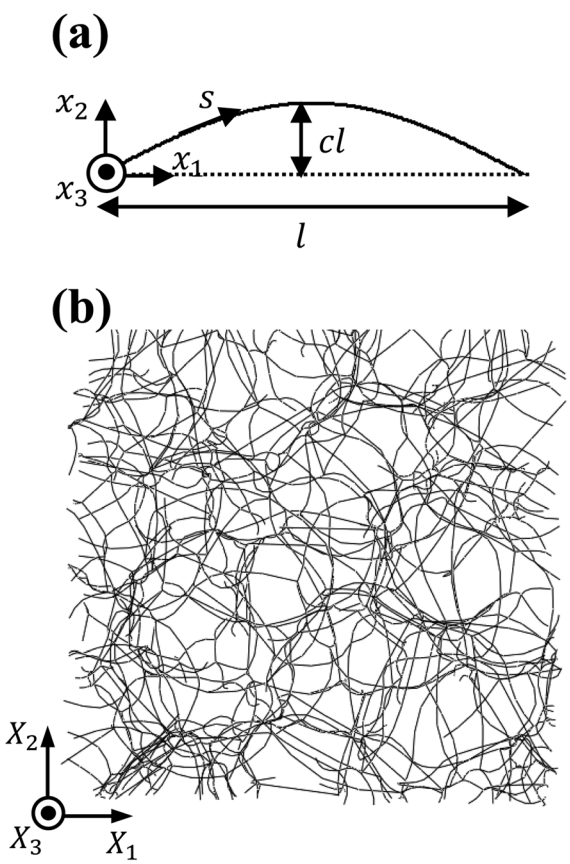

Fig. 1 (*a*) Individual crimped fiber and (*b*) snapshot of an undeformed 3D Voronoi network of 1331 naturally curved fibers. A normalized fiber crimp amplitude $c = 0.2$ ($\tau = 1.14$) is used in both panels.

2 Model and Simulation Method

Random fiber networks are generated using the Voronoi algorithm. A large number (6000) of seed points are randomly positioned in a cube of edge length equal to 1. This volume is then tessellated using the Voronoi procedure. Fibers are defined along all edges of the resulting polyhedra. The vertices of the polyhedra are the cross-links of the network, and the coordination number is 4 at all network interior points. This leads to a network of straight fibers. To introduce crimp, a fraction f of the total number of fibers are selected and their shape is modified into a sinusoidal curve having the same end points as the initial, straight fiber. Only the longest fibers of the model are selected for this purpose. The curve describing a crimped fiber has wavelength $2l$ and amplitude cl, both proportional to the end-to-end distance l. Each crimped fiber belongs to a plane P containing the end-to-end vector of the filament and having random azimuthal angle. In a Cartesian coordinate system with x_1 in the direction of the fiber end-to-end vector and x_2 contained in plane P, the fiber shape is defined by $x_2 = cl\sin(\pi x_1/l)$, as shown schematically in Fig. 1(*a*) for a fiber with $c = 0.2$. The tortuosity, defined as the contour length divided by the end-to-end length, is evaluated as $\tau = 2E_2(-c\pi)/\pi$, where E_2 is the complete elliptic integral of the second kind. This relation gives $\tau = 1.14$ for the normalized amplitude $c = 0.2$. It can be noted that the resulting length of individual fibers l is exponentially distributed, as previously seen in other types of networks [6] and observed in experiments performed on actin gels [20]. Figure 1(*b*) shows a snapshot of such networks with $f = 1$ and $c = 0.2$ ($\tau = 1.14$). It should be noted that the use of the ratio of amplitude-to-wavelength (parameter c, here) as the only parameter capturing the effect of crimp on fiber behavior has been also

suggested in Ref. [21] in the context of a composite with crimped, nonbonded fibers.

Although crimp is induced using a wavelength of $2l$ in all cases, it should be noted that for small values of c, in the axially dominated networks, the configuration shown in Fig. 1(*a*) is also representative of fibers of length nl and crimp amplitude cl, for arbitrary positive integers n. This point is revisited in Sec. 3.1.

In models with matrix, the network is embedded in a continuum which fills the volume of the cubic material domain. The fibers have no associated volume and are represented by beams of axial and bending stiffnesses EA/l and EI/l^3, respectively. The fibers are considered well-bonded to the matrix, and this compatibility condition is imposed along all interfaces. It is important to observe that this structure is different from a regular composite material since the fibers form a percolated cross-linked three-dimensional network within the matrix.

The fibers are represented either as trusses of axial stiffness $(EA)_f/l$ or as two-noded Timoshenko beams, as specified. The fiber material is considered linear elastic. The fiber elastic strain energy is computed as

$$U = \int_0^{l_s} \left[(EI)_f \left(\frac{d\psi(s)}{ds} \right)^2 + (EA)_f \left(\frac{du(s)}{ds} \right)^2 + (GA)_f \left(\frac{dv(s)}{ds} - \psi(s) \right)^2 + (GJ)_f \left(\frac{d\phi(s)}{ds} \right)^2 \right] ds \quad (1)$$

where l_s is the fiber contour length and E, G, A, I, and J are the Young's and shear moduli, cross-sectional area, and the axial and polar moments of inertia, respectively. The beam cross section is considered circular, so the moment of inertia of the cross section, I, is not direction-dependent. Functions $v(s)$, $\psi(s)$, $\phi(s)$, and $du(s)/ds$ represent the transverse displacement, rotation, torsional rotation, and the normal axial strain at position s along the fiber axis, respectively. The use of Timoshenko beams in place of the Euler–Bernoulli model more frequently used in the literature is determined by the superior convergence properties of these models, as discussed in Ref. [8]. In the case of trusses, only the second term remains in the integral. The matrix is considered linear elastic, with Young's modulus E_m and Poisson's ratio ν_m.

This model is discretized using finite elements. All fibers are discretized with four straight beam elements connecting points positioned along the fiber contour. It is verified that using more beam elements per fiber does not modify the results reported here. In the case of the network with matrix, the matrix is considered linear elastic and the matrix and fibers are meshed together, such that the end nodes of a fiber element are shared with the adjacent 3D tetrahedral solid elements. The modeling procedure is identical to that used by Zhang et al. [10]. The 3D and beam/truss elements have the same nodal displacement variables. When using trusses to represent fibers, the interpolation functions used for fibers and matrix elements are of the same order, and hence, the compatibility is ensured everywhere. When using beams to represent fibers, the compatibility is ensured only at the nodal sites. However, the convergence studies for the overall network properties mentioned above indicate that the presence of multiple nodes along each fiber imposes the compatibility of the fiber-matrix deformation to a sufficient degree in all cases studied.

The model is deformed by imposing displacement boundary conditions. A uniaxial strain is applied in the x_1 direction, $\varepsilon_{11} = \epsilon$, while the faces perpendicular to the x_2 and x_3 axes are kept traction free. Displacement is prescribed for the nodes on the model faces with the minimum and maximum x_1 coordinates. The small deformation simulations are performed up to $\epsilon = 0.05\%$ applied strain, while larger strains are used in the other cases, as specified, to investigate the nonlinear deformation range. Shear deformation was also applied in several cases and the results for small deformations (linear elasticity) are in agreement with those obtained from uniaxial tests, as also reported broadly in the literature [3,6,8,9].

The overall Cauchy stress is evaluated based on the reactions computed on the face of normal in the x_1 direction and the current area of the respective model boundary segment. In the case with matrix, these include reactions from fiber and matrix elements. Alternatively, the stress components can be calculated using the strain energy stored in the matrix and network elements.

The solution is obtained using either the commercial finite element solver ABAQUS/STANDARD 6.9-2 or an in-house developed C++ code, which has been extensively tested in previous studies (e.g., see Refs. [10,11]).

3 Results and Discussion

3.1 Fiber Networks Without a Nonfibrillar Matrix. Networks with various values of the two parameters, the fraction of fibers crimped, f, and the crimp amplitude, c, are generated, and multiple realizations are tested for each case. The density, which is controlled by the number of seeds in the Voronoi procedure, is kept constant. The small-strain network modulus, E_N, is evaluated as described in Sec. 2. The case with straight fibers ($f = 0$) is taken as reference and its modulus is denoted by E_{N0}. The axial and bending stiffness parameters of fibers, $(EA)_f$ and $(EI)_f$, are chosen such that the network of straight fibers is in the axial deformation regime. This does not imply that networks with $f > 0$ are deforming in the same mode since bending is engaged under any type of local loading in presence of crimp.

Figure 2(*a*) shows a map of E_N normalized by E_{N0} versus parameters f and c (the corresponding tortuosity, τ, is also indicated). As expected, the modulus decreases monotonically with increasing f and c. Figure 2(*b*) shows several horizontal sections through the map in Fig. 2(*a*), each corresponding to constants $c = 0$, 0.25, 0.5, 0.66, and 1 (from top to bottom). This corresponds to tortuosity values of $\tau = 1$, 1.17, 1.32, 1.40, and 1.56, respectively. Note that the level of tortuosity relevant for collagen networks is on the order of 1.21 [22]. The continuous curve in Fig. 2(*b*) represents a lower bound for the reduction of networks stiffness. It is obtained by considering that all crimped fibers are actually removed from the model (the limit $c \to \infty$) and do not contribute to the global strain energy. The derivation of this analytical bound is provided in the Appendix. This bound is independent of the density and fiber stiffness. The solid curve corresponds to stable networks that are deforming in the axially dominated regime.

In order to provide an approximation of the numerical results presented in Fig. 2, it is useful to establish a connection with our previous results [9]. In this reference, composite networks of straight fibers were considered, in which $(EA)_f$ (or $(EI)_f$) of each fiber was selected from a distribution function of mean $\overline{(EA)_f}$ and standard deviation $\sigma_{(EA)_f}$. Upon considering multiple realizations of such structures, the resulting network moduli formed a distribution of mean $\overline{E_N}$ and standard deviation σ_{E_N}. It was shown that $\overline{E_N}$ decreases as $\sigma_{(EA)_f}$ increases. The upper bound is the value of the modulus corresponding to $\sigma_{(EA)_f} = 0$, i.e., the case in which all fibers of the network have the same axial stiffness, equal to $\overline{(EA)_f}$. It was further discussed in Ref. [9] that σ_{E_N} increases linearly with $\sigma_{(EA)_f}$, but decreases as $N_f^{-0.5}$ with increasing the number of fibers in the model, N_f.

It is possible to link the case discussed here to that analyzed in Ref. [9]. To this end, consider networks that are axially dominated. In these cases, the bending behavior of the fibers is inconsequential for the overall system response. If all fiber segments are straight, $(EA)_f$ is identical for all fibers. In the presence of crimp, the effective axial stiffness decreases with increasing c (or τ). The change in equivalent $(EA)_f$ can be computed analytically using elementary methods for slender curved beams [23]. To this end, Castigliano's second theorem can be used to find the resulting displacement, δ, from the application of an axial unit load p to a

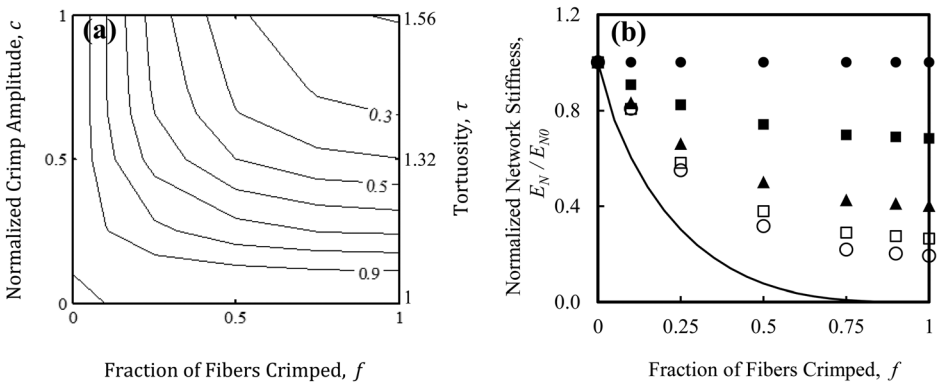

Fig. 2 (*a*) Contour map of the normalized overall network stiffness, E_N, function of the crimp amplitude, *c*, and fraction of crimped fibers, *f*, for networks which are not embedded in matrix. The network stiffness values are normalized by the stiffness of the same network with straight fibers, E_{N0}. (*b*) Data selected from (*a*) for four values of parameter *c*: 0 (filled circles), 0.25 (filled squares), 0.5 (triangles), 0.66 (open squares), and 1 (open circles), corresponding to tortuosity values of $\tau = 1, 1.17, 1.32, 1.40$, and 1.56, respectively. The solid curve represents a lower bound for E_N/E_{N0} predicted for networks in the axially dominated regimes (Appendix).

curved beam. The equivalent axial parameter $(EA)_{\text{eq}}$ can be evaluated as $(EA)_{\text{eq}} = l/(\delta/p)$.

The distribution of $(EA)_{\text{eq}}$ values for fibers of different lengths can then be evaluated considering the distribution of cl. The resulting distribution is characterized by its mean, $\overline{(EA)}_{\text{eq}}$, standard deviation, $\sigma_{(EA)_{\text{eq}}}$, and third central moment M_3.

This observation maps the present case to that of a composite network of straight fibers. The discussion below is an extension of the derivation in Ref. [9] establishing a connection between E_N and the distribution of fiber properties. While the fibers considered in this study have identical material properties and cross sections, a distribution of fiber properties emerges as a result of crimp when explicitly accounting for the distribution of fiber lengths in the network.

If the considered network is in the axial deformation regime after imposing the crimp, E_N is only a function of the parameter, $(EA)_{\text{eq}}$ [6,7,9]. For brevity, $(EA)_{\text{eq}}$ of fiber i is denoted by k_i and $\boldsymbol{k}$ represents the respective fiber stiffness values k_i for the entire network. In the special case where all fibers have the same stiffness k_0, $\boldsymbol{k} = \boldsymbol{k}_0 = k_0\,\mathbf{1}$ and $E_{N0} = E_N(\boldsymbol{k}_0)$. With this notation, one can write the departure, $\boldsymbol{\delta}$, of a generic case where all fibers have different stiffness from the case in which fibers have identical stiffness as $\boldsymbol{\delta} = \boldsymbol{k} - \boldsymbol{k}_0$. E_N can be written as a Taylor series expansion about $\boldsymbol{k}_0$

$$E_N(\boldsymbol{k}) = E_{N0} + \left[(\boldsymbol{\delta}.\nabla_{\boldsymbol{k}})E_N(\boldsymbol{k}) + \frac{1}{2}(\boldsymbol{\delta}.\nabla_{\boldsymbol{k}})^2 E_N(\boldsymbol{k})\right]_{\boldsymbol{k}=\boldsymbol{k}_0} + \cdots \quad (2)$$

In the general case of a random network, $\boldsymbol{k}$ is a stochastic parameter. At small deformations, the variation $\boldsymbol{\delta}$ can be expressed in terms of parameter c (or τ) and is statistically defined by the distribution function of fiber stiffness values. $\boldsymbol{k}$ can be characterized by its mean shift, $\overline{\delta k}$, and its second and third central moments, σ_k^2 and M_3, respectively. Taking the average of Eq. (2), the mean network stiffness results in

$$\overline{E_N} \approx E_{N0} + \overline{\delta k}C_1 + (\overline{\delta k})^2 C_2 + \sigma_k^2 C_3 + (\overline{\delta k})^3 C_4 + \overline{\delta k}\sigma_k^2 C_5 + M_3 C_6 \quad (3)$$

where C_1 to C_6 are constants for a specific network structure. They are related to the derivatives of E_N with respect to k_i. For example, C_1 is the scaling prefactor in the relation $E_N \sim (EA)_f$ known to be valid in the axial deformation regime. If the changes in $\boldsymbol{k}$ are small, one may approximate $E_N \approx E_{N0} + \overline{\delta k}C_1$. Since E_N is linear in $\overline{\delta k}$, this resembles the previously observed scaling laws $E_N \sim (EA)_f$ established for networks of straight fibers. So, coefficient C_1 can be obtained from the variation of the network modulus with $(EA)_f$ in the equivalent network of straight fibers.

Figure 3 shows the comparison of this approximation with the numerical results. The symbols correspond to the variation of E_N/E_{N0} with c for $f = 1$ (Fig. 2(*b*)), and the curves correspond to the approximation of Eq. (3) using terms up to the first-order (continuous line) and third-order (dotted line), respectively. The continuous curve is predicted using a C_1 value obtained from the calculation of E_N versus $(EA)_f$ for the network in the absence of crimp, so the continuous line is predicted. The additional constants in the expansion required to plot the dotted line are fitted. The first-order approximation provides a good fit up to $c = 0.17$ or $\tau = 1.12$. This extends the predictive power of the known

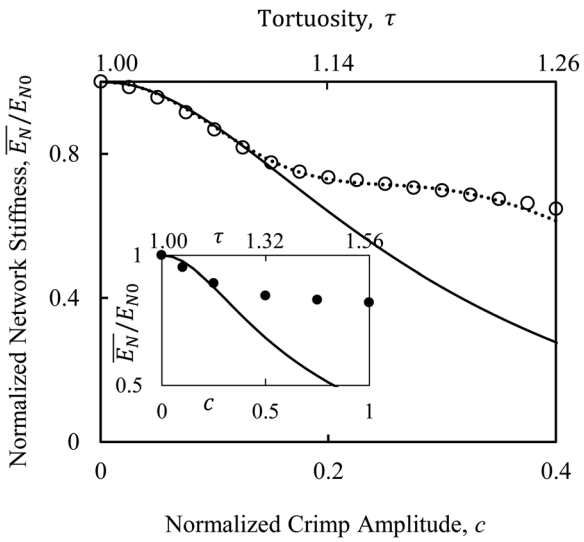

Fig. 3 Estimations for the normalized overall stiffness of a network as a function of the normalized crimp amplitude or tortuosity for the case $f = 1$. The symbols represent data from Fig. 2 for a 3D Voronoi network in the axially dominated regime. The solid line represents the prediction of Eq. (3) truncated to the first-order, while the dashed line represents the fit of Eq. (3) truncated to the third-order. The inset shows the normalized network stiffness of a 2D Voronoi, bending-dominated network (symbols), with the curve being the prediction of Eq. (3) truncated to the first-order.

results for networks of straight fibers to networks of crimped fibers with small and moderate crimp ($c \leq 0.17$ or $\tau \leq 1.12$).

In order to study the bending-dominated case, we test 2D versions of the same system. To this end, we construct 2D Voronoi networks using a procedure similar to that described in Sec. 2 for 3D models. The advantage of using 2D models is that the plane of bending is well-defined, while the bending-dominated cases in 3D are difficult to fit in this framework since a crimped beam subjected to bending has different bending stiffnesses in various planes that share the fiber end-to-end vector. Due to the stochastic loading of the filaments, it is not clear that in all situations, the crimped beams deform in the direction of the smallest $(EI)_{eq}$, and hence, the actual effective bending stiffness of individual fibers is not known. The inset of Fig. 3 shows the results for 2D bending-dominated Voronoi networks. The predictive power of the analogy described above is again obvious, since the continuous line provides a good fit of the numerical data up to $c = 0.25$ ($\tau = 1.17$).

The solution for a curved slender beam shows that in the axially dominated case, $(EA)_{eq} \sim (EA)_f$. On the other hand, for an axially dominated network, E_N varies with fiber density and stiffness according to the scaling laws $E_N \sim \rho$ and $E_N \sim (EA)_f$. So, the suggested series estimate for the variation of E_N/E_{N0} due to crimp is independent of density and fiber stiffness for the axially dominated networks. The same argument holds for the bending-dominated series estimate by noting the scaling laws $(EI)_{eq} \sim (EI)_f$, $E_N \sim (EI)_f$, and $E_N \sim \rho^\alpha$ with α depending on the network type.

Next, the nonlinear response of networks of crimped fibers is tested. It has been previously shown using simulations and experiments that the response of fibrous networks and similar networks of collagen to uniaxial tension and shear is characterized by an initial linear regime followed by power law hardening [3,24]. The variation of the tangent stiffness, E^t, with stress is then described by an initial, small stress/strain regime in which the stiffness is constant, followed by a power law variation of the large strain tangent stiffness with stress. The small stress/strain stiffness depends on the material properties of the fibers. However, all networks have the same tangent stiffness versus stress asymptote at large stresses. It has been shown [9] that composite networks in which each fiber has different material properties behave qualitatively in a similar manner. Here, the same behavior is observed when testing networks of crimped fibers with various c and f values. Figure 4 shows results for systems with $f = 1$ and $c = 0$, 0.3, 0.5, and 0.75 ($\tau = 1.00$, 1.20, 1.32, and 1.45, respectively), and a case with $f = 0.5$ and $c = 0.5$ ($\tau = 1.32$).

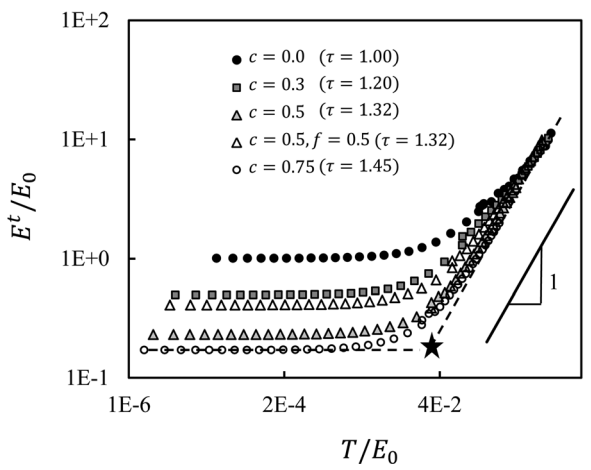

Fig. 4 Normalized tangent stiffness, E^t, against normalized true stress, T, for networks with crimped fibers. Stress and stiffness values are normalized by the stiffness of the network with straight fibers. In all cases, $f = 1$, except as indicated in the legend. The star marks the approximate strain of transition to the hardening regime.

Despite their initial differences, the stiffness against stretch curves converge to a single characteristic curve at large strains. This is in agreement with previous observations of Onck et al. [5] where fiber crimp was also considered explicitly. It can be noted that differences between these systems persist even in the nonlinear range to a fairly large strain before convergence to the asymptote is achieved. The stiffening response of the fiber networks has been characterized by power law dependences of the form $E^t \sim T^\alpha$. α values ranging from 1/2 to 3/2 have been reported depending on network architecture and cross-link properties [3,25]. The stiffening behavior of the tested Voronoi networks is similar to the experimental observations using collagen networks showing $\alpha = 1$ [3]. The data in Fig. 4 indicate further that the critical strain marking the onset of nonlinear behavior, ε_c, is independent of the crimp parameters, and the stress–strain curve in the nonlinear range is described by $T \sim \exp(\varepsilon/\varepsilon_c)$. The critical strain, ε_c, can be evaluated using curves such as those presented in Fig. 4 as the strain corresponding to the intersection of the two asymptotes for the two regimes of constant stiffness and strain stiffening (marked by a star sign in Fig. 4 for the curve $c = 0.75$).

3.2 Networks Embedded in an Elastic Matrix. In many practical cases such as in connective tissue, fiber networks are embedded in a matrix. Hence, it becomes important to determine to what extent the features discussed for the nonembedded networks remain valid in the presence of the matrix. A prominent example of such situations is that of soft tissue composed from collagen fibers and an embedding medium. The mechanics of such materials was studied using explicit, coupled network–matrix models in Refs. [10,11,13]. Here, similar models are used to investigate the effect of crimp. It should be noted that, as for the rest of this study, the results of this section only apply to networks of athermal fibers.

Simulation parameters suggested by Lake et al. [13] calibrated using experimental data for soft tissue collagen are adopted here. $E_f = 6.5$ MPa is used to reproduce stress values observed in experiments using collagen networks. A diameter of 70 nm and a volumetric mass density of 1.34 g/ml are assumed for the individual fibers, and a collagen concentration of about 1 mg/ml is considered for the network. Cubic models with these parameters and with edge sizes of about 26 μm are constructed. To render the model relevant for connective tissue, E_m values in the range 10^{-4} to 10^2 kPa are considered, while a Poisson's ratio of 0.3 is used in all cases. In these models, the parameters c and f are varied from 0 to 0.5 (τ varies from 1.00 to 1.32).

The system taken as most representative for the soft tissue case, with $E_m = 10$ kPa, has almost an affine deformation field. The contribution of the network to the overall stiffness is approximately 20%. As E_m increases to 10^2 kPa and above, the network contributes less to the overall traction and effective stiffness. In this regime, the matrix confines the network deformation and the effect of crimp is minimal. For $f = 0.5$ and $c = 0.5$ ($\tau = 1.32$), E_N of the crimped network is only 2% different from the stiffness of the network of straight fibers of the same parameters embedded in the same matrix. Further tests indicate that the effect stays negligible even for collagen network concentrations as high as 50 mg/ml.

To reach a regime in which the network signature is visible in the overall behavior, the matrix modulus has to be reduced to $E_m = 10^{-4}$ kPa, which is significantly smaller than the stiffness of soft tissue [26] and structural biomaterials [27]. In this case, the deformation becomes more nonaffine. Consequently, the effect of crimp is significantly stronger than seen in the systems with larger E_m. The normalized E_N from these tests is shown in Fig. 5(*a*). For $f = 0.5$ and $c = 0.5$ ($\tau = 1.32$), E_N of the crimped network is about 5% smaller than the stiffness of the network of straight fibers of same parameters. Clearly, the effect of crimp on modulus

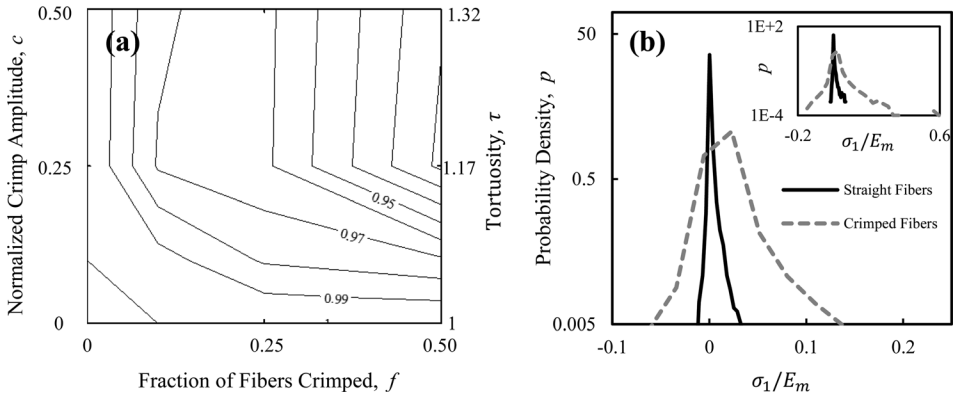

Fig. 5 (*a*) Contour map of the normalized sample stiffness, E_N, for different normalized crimp amplitudes, c, and fractions of crimped fibers, f, for network of fibers embedded in an elastic matrix. The network stiffness values are normalized by the stiffness of systems with straight fibers. The matrix stiffness is $E_m = 10^{-4}$ kPa. The network parameters are indicated in the text. (*b*) Section of the probability density function of the normalized maximum principal stress in the matrix, σ_1. The full range of this distribution is shown in the inset. This set of data corresponds to a network with $c = 0.25$ ($\tau = 1.17$) and $f = 1$. These values are normalized by the matrix stiffness of 10^{-2} kPa.

is much smaller in presence of the matrix compared to the case of the network without matrix (Fig. 2(*a*)).

As discussed, the matrix forces the network to deform more affinely. This constraint leads to large interaction forces which lead to an increase of the stress in the matrix. The effect is more pronounced in the presence of crimp. This is shown for a system with $E_m = 10^{-2}$ kPa in Fig. 5(*b*), showing the probability distribution function of the maximum principal stress in the matrix (all elements of the matrix have been sampled) for a system with straight fibers and the same system with crimped fibers with $c = 0.25$ ($\tau = 1.17$) and $f = 1$. The distribution corresponding to the crimped fiber system is much broader than the reference distribution (continuous line), which quantifies the statement made above. Therefore, it is concluded that the crimp does not significantly change the stress–strain curve of the network–matrix system, but makes damage nucleation in the matrix more probable.

4 Conclusions

The effect of fiber crimp on the linear and nonlinear elasticity of fiber networks is investigated. Both networks embedded in matrix and networks without matrix are considered. In the case of the networks without matrix, the small-strain elastic modulus decreases rapidly with the crimp amplitude and the fraction of crimped fibers in the model. This decrease is approximated using a model based on an equivalence between a network of crimped fibers and a network of straight fibers, in which the material properties of each fiber are different. This semi-analytic approximation allows predicting the effect of crimp up to crimp amplitudes as high as $c = 0.17$ based exclusively on results from fiber network theory. The effect of crimp disappears gradually under large deformations, but persists into the nonlinear range up to significant strains.

An embedding matrix confines the network to deform more affinely. This renders the effect of fiber crimp very small relative to the network of straight fibers case, even when very small matrix stiffnesses are considered. However, large stresses result in the matrix due to the network–matrix interaction and their magnitude increases with increasing crimp. This indicates that matrix damage initiation should be easier in embedded networks with crimp compared with the same systems without crimp. The understanding gained in this work is relevant for many physical systems, including the deformation of connective tissue, carbon nanotube-based 2D and 3D network structures, and various types of nonwovens.

Acknowledgment

E.B. gratefully acknowledges Abouzar Ghavami at RPI for fruitful discussion and Lijuan Zhang and Ali Shahsavari at RPI for fruitful discussions and help with finite element simulations. The authors also gratefully acknowledge the financial support of the National Institute of Health (Grant Nos. NIH-R01-EB005813 and NIH-U01-EB016638).

Appendix: Lower Bound Estimation for the Effect of Crimp on the Small-Strain Modulus. A lower bound can be established for the fiber networks modulus based on removing the curved fibers. The change in the density of fibers, ρ, is calculated due to the removal of a certain fraction of the fibers that are longer, f. Then, the asymptotic scaling laws relating the overall stiffness to ρ are used to estimate the change in E_N as a function of f. This estimation is expected to be accurate in dense networks where removing fibers would not result in loss of percolation.

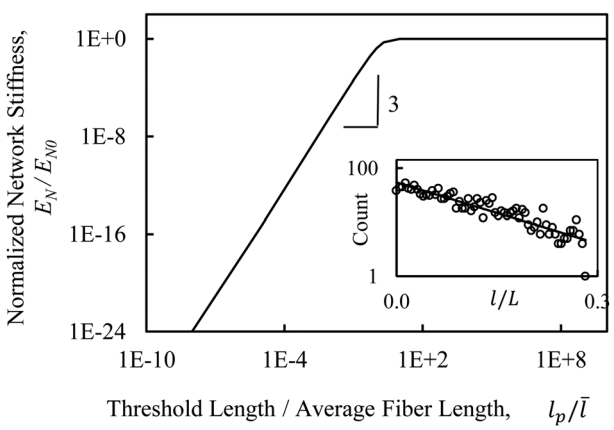

Fig. 6 Scaling of normalized network stiffness against curving threshold length, l_p, divided by the average fiber length, $\bar{l}$ using the fiber removing model. The network stiffness values are normalized by the stiffness of networks with straight fibers. The inset shows the exponential normalized fiber length distribution in a network. The fiber length is normalized by the dimension of the simulated networks, L.

Exponential distribution of fiber length is considered as shown in the inset of Fig. 6, $p(l) = \bar{l}^{-1} \exp(-l/\bar{l})$, where $\bar{l}$ is the average fiber length. Removing a fraction of fibers f results in the removal of fibers longer than a threshold length, l_p. The fiber length distribution relates l_p to f as $l_p = -\bar{l}\ln(f)$. If all fibers longer than l_p are removed, the new average fiber length can be calculated using a truncated form of the fiber length distribution as

$$\bar{l}^* = \bar{l}[1 - (1 - \ln(f))f] \tag{A1}$$

Hence, the new total fiber length is $(1-f)\bar{l}^*$. On the other hand, it is observed that $E_N \sim \rho^\alpha$ with $\alpha = 1$ and 2 in the stretch- and bending-dominated Voronoi beam networks. Using the relations between ρ and f and assuming stretch-dominated deformation yield

$$E_N \sim (1-f)[1 - (1 - \ln(f))f] \tag{A2}$$

This estimate is shown using the solid line in Fig. 2(*b*). Assuming a bending-dominated fiber deformation squares, the estimated E_N considering the exponent $\alpha = 2$ for the Voronoi network.

Additionally, rewriting Eq. (A2) in terms of l_p yields

$$E_N \sim (1 - e^{-l_p/\bar{l}})[1 - e^{-l_p/\bar{l}}(1 + l_p/\bar{l})] \tag{A3}$$

Figure 6 shows normalized E_N plotted for different $l_p/\bar{l}$ ratios calculated using Eq. (A3) at values lying on the two sides of $l_p/\bar{l} = 1$. A power law scaling $E_N \sim (l_p/\bar{l})^3$ is observed for $l_p < \bar{l}$ in the vicinity of $l_p/\bar{l} = 1$.

References

[1] Picu, R. C., 2011, "Mechanics of Random Fiber Networks—A Review," Soft Matter, **7**(15), pp. 6768–6785.

[2] Broedersz, C., and MacKintosh, F., 2014, "Modeling Semiflexible Polymer Networks," Rev. Mod. Phys., **86**(3), pp. 995–1036.

[3] Licup, A., Munster, S., Sharma, A., Sheinman, M., Jawerth, L., Fabry, B., Weitz, D., and MacKintosh, F., 2015, "Stress Controls the Mechanics of Collagen Networks," Proc. Natl. Acad. Sci. U. S. A., **112**(31), pp. 9573–9578.

[4] van Dillen, T., Onck, P., and Van der Giessen, E., 2008, "Models for Stiffening in Cross-Linked Biopolymer Networks: A Comparative Study," J. Mech. Phys. Solids, **56**(6), pp. 2240–2264.

[5] Onck, P., Koeman, T., van Dillen, T., and Van der Giessen, E., 2005, "Alternative Explanation of Stiffening in Cross-Linked Semiflexible Networks," Phys. Rev. Lett., **95**(17), pp. 178102–178105.

[6] Shahsavari, A., and Picu, R. C., 2013, "Elasticity of Sparsely Cross-Linked Random Fibre Networks," Philos. Mag. Lett., **93**(6), pp. 356–361.

[7] Broedersz, C. P., Mao, X., Lubensky, T. C., and MacKintosh, F. C., 2011, "Criticality and Isostaticity in Fibre Networks," Nat. Phys., **7**(12), pp. 983–988.

[8] Shahsavari, A., and Picu, R. C., 2012, "Model Selection for Athermal Cross-Linked Fiber Networks," Phys. Rev. E, **86**(1), p. 011923.

[9] Ban, E., Barocas, V. H., Shephard, M., and Picu, R. C., 2015, "Softening in Random Networks of Non-Identical Beams," J. Mech. Phys. Solids, **87**, pp. 38–50.

[10] Zhang, L., Lake, S., Barocas, V. H., Shephard, M. S., and Picu, R. C., 2013, "Cross-Linked Fiber Network Embedded in an Elastic Matrix," Soft Matter, **9**(28), pp. 6398–6405.

[11] Zhang, L., Lake, S., Lai, V., Picu, R. C., Barocas, V. H., and Shephard, M. S., 2013, "A Coupled Fiber-Matrix Model Demonstrates Highly Inhomogeneous Microstructural Interactions in Soft Tissues Under Tensile Load," ASME J. Biomech. Eng., **135**(1), p. 011008.

[12] Cacho, F., Elbischger, P., Rodríguez, J., Doblaré, M., and Holzapfel, G., 2007, "A Constitutive Model for Fibrous Tissues Considering Collagen Fiber Crimp," Int. J. Nonlinear Mech., **42**(2), pp. 391–402.

[13] Lake, S., Hadi, M., Lai, V., and Barocas, V. H., 2012, "Mechanics of a Fiber Network Within a Non-Fibrillar Matrix: Model and Comparison With Collagen-Agarose Co-Gels," Ann. Biomed. Eng., **40**(10), pp. 2111–2121.

[14] Legerlotza, K., Dornb, J., Richtera, J., Rauschc, M., and Leupin, O., 2014, "Age-Dependent Regulation of Tendon Crimp Structure, Cell Length and Gap Width With Strain," Acta Biomater., **10**(10), pp. 4447–4455.

[15] Franchi, M., Raspanti, M., Dell'Orbo, C., Quaranta, M., De Pasquale, V., Ottani, V., and Ruggeri, A., 2008, "Different Crimp Patterns in Collagen Fibrils Relate to the Subfibrillar Arrangement," Connect. Tissue Res., **49**(2), pp. 85–91.

[16] Raina, A., and Linder, C., 2014, "A Homogenization Approach for Nonwoven Materials Based on Fiber Undulations and Reorientation," J. Mech. Phys. Solids, **65**, pp. 12–34.

[17] Kabla, A., and Mahadevan, L., 2007, "Nonlinear Mechanics of Soft Fibrous Networks," J. R. Soc., Interface, **4**(12), pp. 99–106.

[18] Huisman, E., van Dillen, T., Onck, P., and Van der Giessen, E., 2007, "Three-Dimensional Cross-Linked F-Actin Networks: Relation Between Network Architecture and Mechanical Behavior," Phys. Rev. Lett., **99**(20), pp. 208103–208106.

[19] Wen, Q., Basu, A., Janmey, P., and Yodh, A., 2012, "Non-Affine Deformations in Polymer Hydrogels," Soft Matter, **8**(31), pp. 8039–8049.

[20] Janmey, P., Peetermans, J., Zaner, K. S., Stossel, T. P., and Takana, T., 1986, "Structure and Mobility of Actin Filaments as Measured by Quasielastic Light Scattering, Viscometry, and Electron Microscopy," J. Biol. Chem., **261**(18), pp. 8357–8362

[21] Hsiao, H., and Daniel, I., 1996, "Effect of Fiber Waviness on Stiffness and Strength Reduction of Unidirectional Composites Under Compressive Loading," Compos. Sci. Technol., **56**(5), pp. 581–593.

[22] Lai, V., Frey, C., Kerandi, A., Lake, S., Tranquillo, R., and Barocas, V. H., 2013, "Microstructural and Mechanical Differences Between Digested Collagen-Fibrin Co-Gels and Pure Collagen and Fibrin Gels," Acta Biomater., **8**(11), pp. 4031–4042.

[23] Love, A., 1944, *A Treatise on the Mathematical Theory of Elasticity*, Dover Publications, New York.

[24] Zagar, G., Onck, P., and Van der Giessen, E., 2011, "Elasticity of Rigidly Cross-Linked Networks of Athermal Filaments," Macromolecules, **44**(17), pp. 7026–7033.

[25] Zagar, G., Onck, P., and Van der Giessen, E., 2015, "Two Fundamental Mechanisms Govern the Stiffening of Cross-Linked Networks," Biophys. J., **108**(6), pp. 1470–1479.

[26] Discher, D., Mooney, D., and Zandstra, P., 2009, "Growth Factors, Matrices, and Forces Combine and Control Stem Cells," Science, **324**(5935), pp. 1673–1677.

[27] Barthelat, F., 2007, "Biomimetics for Next Generation Materials," Phil. Trans. R. Soc. A, **365**(1861), pp. 2907–2919.